Optically accessible electrostatic trap for cold polar molecules

Zhenxia Wang, Zhenxing Gu, Yong Xia, Xiang Ji, and Jianping Yin*

State Key Laboratory of Precision Spectroscopy, Department of Physics, East China Normal University, Shanghai 200062, China
**Corresponding author: jpyin@phy.ecnu.edu.cn*

Received March 28, 2013; revised July 1, 2013; accepted July 16, 2013;
posted July 19, 2013 (Doc. ID 187937); published August 7, 2013

We propose an optically accessible electrostatic trap scheme to confine cold polar molecules by using two charged spherical electrodes, and we calculate the corresponding electric field distribution and the Stark trapping potential for ND_3 molecules. We also propose a desirable scheme to realize an efficient loading of cold polar molecules in weak-field-seeking states, and our simulated results show that the maximal loading efficiency can reach ~14%. In addition, we briefly discuss some potential applications of our proposed trap scheme in the studies of optical-potential evaporative cooling and electrostatic surface traps for cold polar molecules.

OCIS codes: (020.0020) Atomic and molecular physics; (020.6580) Stark effect.
http://dx.doi.org/10.1364/JOSAB.30.002348

1. INTRODUCTION

In recent years, more and more research groups have become interested in cold or ultracold molecules and have developed various techniques, such as buffer gas cooling [1,2], photoassociation [3,4], Feshbach resonances [5,6], Stark decelerators [7,8], velocity filters [9,10], laser cooling [11,12], and traps with external (electrostatic, magnetic, optical) fields [13–15], to prepare and manipulate cold molecules, which offer us an opportunity to study high-resolution spectroscopy [16,17], cold collisions [18,19] and cold chemistry [20], quantum computing and quantum information processing [21], and so on. Since the first electrostatic trap for ammonia molecules in weak-field-seeking (WFS) states was realized experimentally by Meijer's group in 2000 [13], some other electric traps for cold polar molecules have been proposed and developed. For example, an ac electric trap for cold molecules in both WFS and strong-field-seeking states was demonstrated by Meijer's group in 2005 [22]. Later they developed a versatile electrostatic trap with the same setup, including dipole trap, quadrupole trap and hexapole trap by applying different voltages to the electrodes. In this experiment, when different dipole terms are added, a hexapole trap can transform into a double-well or donut-shaped trap [23]. In 2007, a half-opened linear ac trap for cold molecules in strong-field-seeking states was demonstrated [24], and its acceptance is small enough to be combined with the Stark decelerator. With its open geometry, one can use laser beams to detect and manipulate the trapped cold molecules. In the same year, Kleinert *et al.* proposed a thin-wire electrostatic trap and successfully trapped ultracold polar NaCs molecules [25].

However, most of the electric traps are complex in geometry, which results in some inconvenience for experimental operations. In particular, their optical accesses are nearly closed, except for the half-opened linear ac trap [24], so it is hard to manipulate and probe the trapped molecules with laser beams. In this paper, we propose a novel electrostatic trap with a simple structure and nearly completely open optical access for cold polar molecules in WFS states, and we calculate the corresponding electrostatic field distribution. Also, we study the dependences of the loading efficiency of cold molecules on both the central velocity of an incident Stark-slowed ND_3 beam and the loading time using a Monte Carlo method, and we discuss some potential applications of our proposed trap.

2. TRAP SCHEME AND FORMULA DERIVATION

Our trap scheme is composed of two charged spherical electrodes with a radius of r_e, as shown in Fig. 1. The distance between the centers of the two spheres is d, while the two thin wires connected to the two spheres are used for applying voltages, and the potential at infinity is 0. It is clear that our scheme is an nearly completely opened optical-access trap, which can be used to form several kinds of electrostatic trap for polar molecules by adding two plate electrodes, laser beams, or substrates (see the brief discussions in Section 4).

We derive a set of analytical solutions to calculate the electrostatic field produced by the two charged spherical electrodes with the same positive high voltage U. Since the wires connected to the spherical electrodes are very thin, we can neglect their influence on the electric field near the origin of Cartesian coordinate system in the following derivation for simplicity. According to the method of image charges, as shown in Fig. 1(b), O_1 and O_2 are the centers of the two electrodes, respectively, while O_3 and O_4 are their first-order image points, where $b(=r_e^2/d)$ is the distance between O_1 and O_4 (or O_2 and O_3). We assume that when the positive voltage U is applied to the two electrodes, the charge on the electrodes are both q, and the charge at the image points O_3 and O_4 are $Q_3 = Q_4 = -q \times (r_e/d)$, while $Q_1 = Q_2 = q + q \times (r_e/d)$

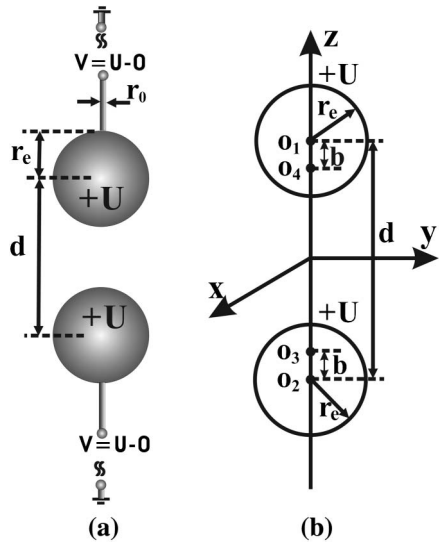

Fig. 1. (a) Schematic diagram of electrostatic trap with two charged spherical electrodes. The radius of the sphere is r_e, and the distance between the centers of the two spheres is d. A positive voltage is applied to the two spheres, and the potential at infinity is 0. (b) Double-sphere layout from the method of images (i.e., the method of image charges). Here O_1 and O_2 are the centers of the two spherical electrodes, respectively, while O_3 and O_4 are their image points, where b is the distance between O_1 and O_4 (or O_2 and O_3).

(Q_1 and Q_2 are the charge at O_1 and O_2, respectively). The electric field generated by the two charged electrodes is approximately equal to that produced by the four charges at O_1, O_2, O_3, and O_4, so we can estimate the electric field distribution of the trap layout in the z direction by

$$E_z = \frac{1}{4\pi\varepsilon_0}\left(\frac{\left(q+\frac{r_e}{d}q\right)\times\left(z+\frac{d}{2}\right)}{\left[x^2+y^2+\left(z+\frac{d}{2}\right)^2\right]^{\frac{3}{2}}}+\frac{\left(q+\frac{r_e}{d}q\right)\times\left(z-\frac{d}{2}\right)}{\left[x^2+y^2+\left(z-\frac{d}{2}\right)^2\right]^{\frac{3}{2}}}\right.$$
$$\left.+\frac{\left(-\frac{r_e}{d}q\right)\times\left[z-\left(-\frac{d}{2}+b\right)\right]}{\left\{x^2+y^2+\left[z-\left(-\frac{d}{2}+b\right)\right]^2\right\}^{\frac{3}{2}}}+\frac{\left(-\frac{r_e}{d}q\right)\times\left[z-\left(\frac{d}{2}-b\right)\right]}{\left\{x^2+y^2+\left[z-\left(\frac{d}{2}-b\right)\right]^2\right\}^{\frac{3}{2}}}\right)$$
$$=\frac{q}{4\pi\varepsilon_0}A'(x,y,z), \tag{1}$$

where ε_0 is the vacuum permittivity. In order to obtain the relationship between the voltage U and the charge q, we calculate the integral of E_z from $r_e + d/2$ to ∞,

$$\int_{\frac{d}{2}+r_e}^{\infty} E_z \mathrm{d}z = \frac{q}{4\pi\varepsilon_0}\int_{\frac{d}{2}+r_e}^{\infty} A'(x,y,z)\mathrm{d}z = U. \tag{2}$$

We assume

$$A = \int_{\frac{d}{2}+r_e}^{\infty} A'(x,y,z)\mathrm{d}z. \tag{3}$$

Once the values of r_e, d, and U are given, the integral A in Eq. (3) can be figured out. For example, when $r_e = 4$ mm, $d = 20$ mm, and $U = 10$ kV, we can obtain $A \approx 299.713$. Therefore, the relationship between the voltage U and charge q can be given by

$$\frac{q}{4\pi\varepsilon_0} = \frac{U}{A}. \tag{4}$$

With Eq. (4), the analytical solutions to calculate the electric field in free space can be approximately expressed as

$$E_x = \frac{U}{A}\left(\frac{\left(1+\frac{r_e}{d}\right)\times x}{\left[x^2+y^2+\left(z+\frac{d}{2}\right)^2\right]^{\frac{3}{2}}}+\frac{\left(1+\frac{r_e}{d}\right)\times x}{\left[x^2+y^2+\left(z-\frac{d}{2}\right)^2\right]^{\frac{3}{2}}}\right.$$
$$\left.+\frac{\left(-\frac{r_e}{d}\right)\times x}{\left\{x^2+y^2+\left[z-\left(-\frac{d}{2}+b\right)\right]^2\right\}^{\frac{3}{2}}}+\frac{\left(-\frac{r_e}{d}\right)\times x}{\left\{x^2+y^2+\left[z-\left(\frac{d}{2}-b\right)\right]^2\right\}^{\frac{3}{2}}}\right), \tag{5}$$

$$E_y = \frac{U}{A}\left(\frac{\left(1+\frac{r_e}{d}\right)\times y}{\left[x+y^2+\left(z+\frac{d}{2}\right)^2\right]^{\frac{3}{2}}}+\frac{\left(1+\frac{r_e}{d}\right)\times y}{\left[x^2+y^2+\left(z-\frac{d}{2}\right)^2\right]^{\frac{3}{2}}}\right.$$
$$\left.+\frac{\left(-\frac{r_e}{d}\right)\times y}{\left\{x^2+y^2+\left[z-\left(-\frac{d}{2}+b\right)\right]^2\right\}^{\frac{3}{2}}}+\frac{\left(-\frac{r_e}{d}\right)\times y}{\left\{x^2+y^2+\left[z-\left(\frac{d}{2}-b\right)\right]^2\right\}^{\frac{3}{2}}}\right), \tag{6}$$

$$E_z = \frac{U}{A}\left(\frac{\left(1+\frac{r_e}{d}\right)\times\left(z+\frac{d}{2}\right)}{\left[x^2+y^2+\left(z+\frac{d}{2}\right)^2\right]^{\frac{3}{2}}}+\frac{\left(1+\frac{r_e}{d}\right)\times\left(z-\frac{d}{2}\right)}{\left[x^2+y^2+\left(z-\frac{d}{2}\right)^2\right]^{\frac{3}{2}}}\right.$$
$$\left.+\frac{\left(-\frac{r_e}{d}\right)\times\left[z-\left(-\frac{d}{2}+b\right)\right]}{\left\{x^2+y^2+\left[z-\left(-\frac{d}{2}+b\right)\right]^2\right\}^{\frac{3}{2}}}+\frac{\left(-\frac{r_e}{d}\right)\times\left[z-\left(\frac{d}{2}-b\right)\right]}{\left\{x^2+y^2+\left[z-\left(\frac{d}{2}-b\right)\right]^2\right\}^{\frac{3}{2}}}\right), \tag{7}$$

$$E = \sqrt{E_x^2+E_y^2+E_z^2}. \tag{8}$$

3. THEORETICAL CALCULATION AND RESULTS

With Eqs. (5)–(8), we calculate the contour distributions of the electric field in xoy, and $xoz(yoz)$ planes for $r_e = 4$ mm, $d = 20$ mm, and $U = 10$ kV, and the results are shown in Figs. 2(a) and 2(c). We find that there is a three-dimensional (3D) closed hollow electrostatic field distribution at the origin (0,0,0) of the Cartesian coordinates, which can be used to trap cold polar molecules in WFS states. Also, we perform the numerical simulation on the contour distributions by using a commercially finite-element software with the same parameters ($r_e = 4$ mm, $d = 20$ mm and $U = 10$ kV), and the results are shown in Figs. 2(b) and 2(d). In the numerical simulation, we consider the influence of the two charged thin wires with a radius of $r_0 = 0.5$ mm and a length of 10 mm, and we set a grounded spherical shell with a radius of R outside the two electrodes, which provides a boundary condition that the potential at physical infinity is equal to 0. Here we set $R = 200$ mm, which is much larger than $r_e + d/2 = 14$ mm ($r_e = 4$ mm and $d = 20$ mm), so the grounded spherical shell can be approximately considered at physical infinity, and the potential is 0. Comparing Fig. 2(a) with 2(b) and Fig. 2(c) with 2(d), we can find that our numerical results are nearly consistent with the analytical ones. This shows that although the influence of the two charged thin wires is not considered in the analytical solutions, the derived Eqs. (5)–(8) can be still used to approximately calculate the electric field distribution of the charged double-sphere trap within $r = 5$ mm.

Afterward, we calculate the spatial distributions of the electrostatic field in x, y, and z directions, and study the dependences of the electric field strength on both the radius r_e and the distance d between the two spherical centers, and the

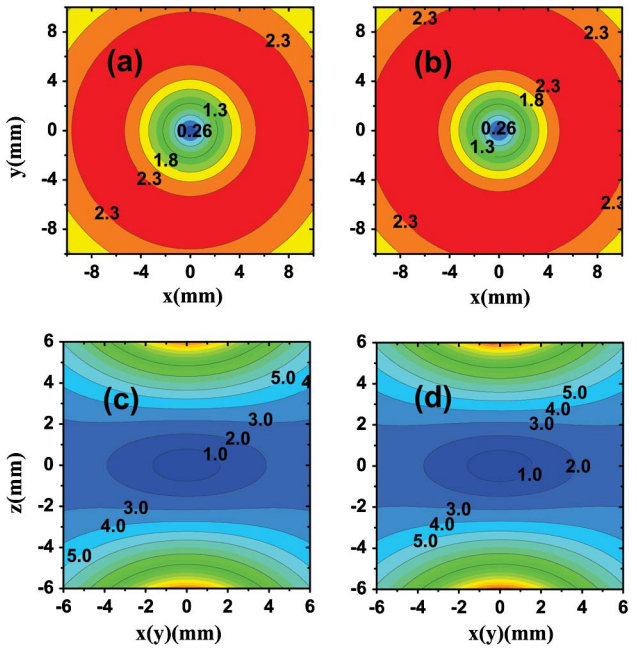

Fig. 2. Contour distributions of the electrostatic field generated by the two charged spheres in xoy and xoz (or yoz) planes for $r_e = 4$ mm, $d = 20$ mm and $U = 10$ kV. (a), (c) Calculated results from our analytical solutions [i.e., Eqs. (5)–(8)]. (b), (d) Numerically calculated distributions from a commercially finite-element software. The labels in the figures are all in unit of kV/cm.

results are shown in Figs. 3(a) and 3(b) and Figs. 3(c) and 3(d), respectively. It is clear that (1) our proposed double-sphere trap is an electrostatic quadrupole one with a central zero electric field and a nearly linear field profile within about $r = 4$ mm, which can be used to trap cold polar molecules in WFS states. (2) The electric field strength on the surface of the electrodes along the z axis is much larger than that at the trap barrier in x and y directions. (3) With the increase of the radius r_e, the maximum electric field strength in x and y directions increases, while that in the z direction decreases. (4) With the increase of the distance d, the effective well depth in x and y directions decreases, while that on the z axis increases. From these dependences, we can find that if the spacing between the two spherical centers decreases or the spherical radius increases, the trap becomes deeper. So we study the dependence of the effective well depth in the three directions on the ratio (r_e/d) of the spherical radius r_e to the distance d, and we find that when $r_e/d = 0.35$, the effective well depths in x, y, and z directions are nearly the same. Figure 4 shows that the smaller r_e is, the deeper the trap is for $r_e/d = 0.35$. In particular, when $r_e = 5$ mm, the effective trapping depth in x, y, and z directions are all about 80 mK, while the optical access is greatly reduced. In order to obtain an electrostatic trap with both nearly completely opened optical access and a deeper trap depth, we need to choose proper trap parameters to form a desirable electrostatic trap. Here we choose $r_e = 4$ mm, $d = 20$ mm, and $U = 10$ kV.

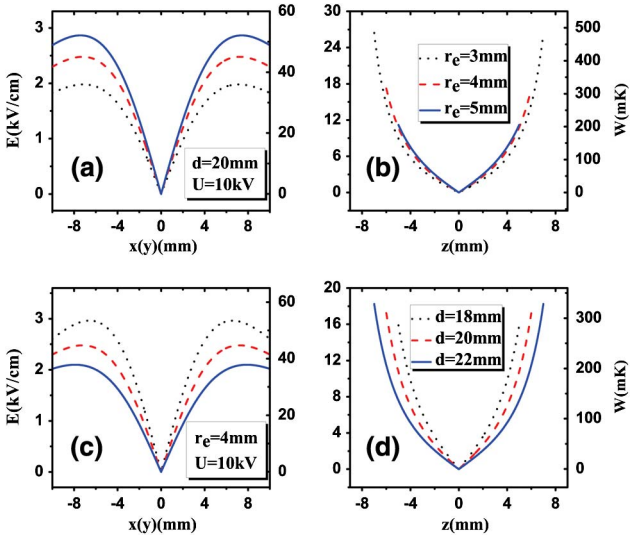

Fig. 3. Spatial distributions of the electrostatic field generated by the two charged spheres and the Stark trapping potential for ND_3 molecules in the three directions for the different spherical radius r_e, when $d = 20$ mm and $U = 10$ kV, and the different distance d between the two spherical centers, when $r_e = 4$ mm and $U = 10$ kV, where (a) and (c) are in the $x(y)$ direction, (b) and (d) are in the z direction.

However, suppose that the two spherical electrodes are punched with a hole with a diameter of d_{hole} along the z axis, as shown in Fig. 5(a). The trap parameters are $r_e = 3.3$ cm, $d = 10$ cm, $U = 50$ kV, and $d_{\text{hole}} = 1$ cm. We can see from Fig. 5(b) that, compared to the scheme of two solid balls (blue dashed–dotted line), the maximum electric field in the z direction of the scheme of two balls with holes (red dashed lines) is much smaller, while the field distributions in the $x(y)$ direction (black solid line) for the two schemes overlap. In this case, not only are the effective trap depths in the three directions nearly the same, but also the optical access of our trap is nearly completely opened when laser beams are propagated along x, y, and z axes.

Finally, we assume that the cold ND_3 molecules come from a Stark decelerated molecular beam in a single WFS state of $|J, K, M\rangle = |1, 1, -1\rangle$, and we calculate the corresponding Stark trapping potential, which can be approximately given by [23]

$$W_{\text{Stark}} = \sqrt{\left(\frac{W_{\text{inv}}}{2}\right)^2 + \left(-\mu E \frac{KM}{J(J+1)}\right)^2} - \left(\frac{W_{\text{inv}}}{2}\right), \qquad (9)$$

where W_{inv} is the inversion splitting and μ is the electric dipole moment of the trapped molecules. The inversion splitting W_{inv} (1.43 GHz) of ND_3 is far smaller than that of NH_3 (23.7 GHz) [23,26]. The results are also shown in Fig. 3. We can see that when $r_e = 4$ mm, $d = 20$ mm and $U = 10$ kV, the efficient Stark trapping potential for ND_3 molecules in

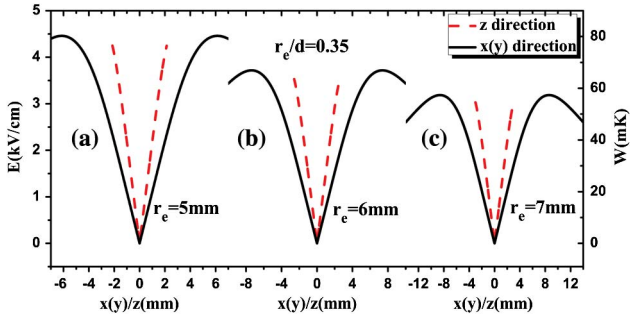

Fig. 4. Dependence of the effective trap depth on the spherical radius r_e for $r_e = 5$ mm (a), 6 mm (b), and 7 mm (c) when $r_e/d = 0.35$, and the maximum electric field in x and y directions are nearly equal to the one in the z direction.

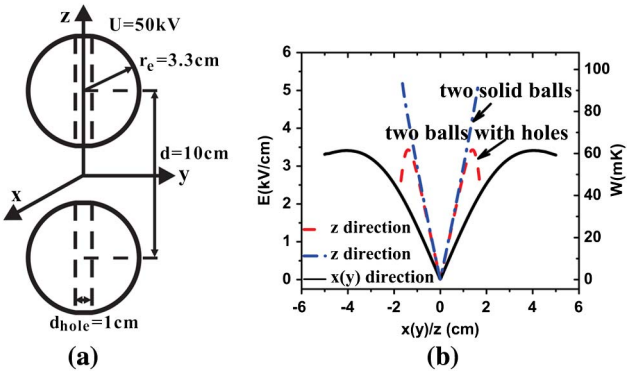

Fig. 5. (a) Scheme of the electrostatic trap with the same well depth and completely opened optical access, which is composed of two spheres with a central hole in the z axis; the optical accesses are along x, y, and z directions, and the trap parameters are $r_e = 3.3$ cm, $d = 10$ cm, $d_{\text{hole}} = 1$ cm, and $U = 50$ kV, respectively. (b) Distributions of the electrostatic field and Stark trapping potentials in the z direction for the schemes of two balls with cylindrical holes (red dashed lines) and two solid balls (blue dashed–dotted line), while the field distributions in the $x(y)$ direction (solid black line) for the two schemes overlap.

x (or y) and z directions are 45 and 300 mK, respectively (red dashed lines), which are high enough to trap cold ND_3 molecules with a temperature of ~20 mK generated by an electrostatic Stark decelerator in our group. Furthermore, we also calculate the first-order derivative of the electrostatic field generated by our charged double-sphere trap and the Stark gradient force on ND_3 molecules, and we find that the corresponding maximum gradient force near the trapping center is far greater than the gravity of ND_3 molecules by about 3 orders of magnitude. This shows that our proposed double-sphere scheme can be used to trap cold ND_3 molecules in the gravity field.

4. SOME POTENTIAL APPLICATIONS AND DISCUSSIONS

A. Loading and Trapping of Cold Molecules

To realize an efficient loading and trapping of cold polar molecules from a pulsed molecular beam, as shown in Fig. 6(a), we add a pair of plate electrodes (8 mm × 8 mm × 0.5 mm) to our double-sphere trap scheme in the y direction (i.e., the direction of the incident molecular beam), and the distance between the two plate electrodes is 16 mm. In order to load the molecules into the trap, a hole with a radius of 2 mm is drilled in the center of the left plate electrode having a high voltage of U_2, while the right plate electrode is grounded. For $r_e = 4$ mm, $d = 16$ mm, $U_1 = 10$ kV, and $U_2 = 9$ kV, we calculate the field distributions in the y direction, and the corresponding contour distributions and the results are shown in the left-hand part of Fig. 6(b). When $U_2 = 0$ and other parameters are unchanged, the results are shown in the right-hand part of Fig. 6(b). We find that when $U_2 = 9$ kV, the left-hand peak of our original double-peak distribution of the electrostatic field generated by the charged double-sphere layout is lowered to nearly zero, and the molecules are decelerated by the gradient force of electrostatic field until most of them are slowed to 0 m/s near the center of the trap. At that very moment, we immediately change the voltage U_2 on the left-hand plate electrode to be grounded to confine the cold molecules in the trap.

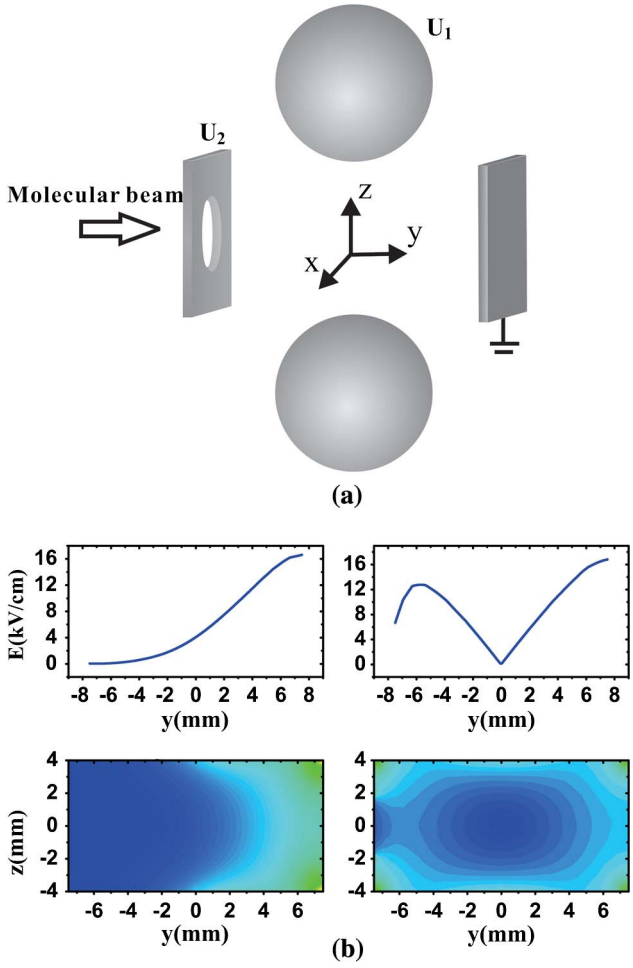

Fig. 6. (a) Schematic diagram of the double-sphere combined with double-plate trap used for efficient loading of cold molecules, and (b) the corresponding electric field profiles in the y direction and the contour distributions in yoz plane for loading (when $U_2 = 9$ kV) and trapping (when $U_2 = 0$) of cold polar molecules, respectively.

In order to check the feasibility of our trap scheme, we perform classical Monte Carlo simulations for the dynamical loading and trapping processes of cold ND_3 molecules. The simulated molecular number is $N = 10^5$, and we assume that the initial spatial distributions and velocity profiles of incident pulsed ND_3 molecular beam are both Gaussian ones, and the transverse and longitudinal spatial sizes are 4 and 8 mm, respectively, and the full-width at half-maximum (FWHM) of the velocity distributions in x, y, and z directions are all 3 m/s. We select a molecule and load it into our trap; with Newton's equations of motion, we can obtain the velocity and position of the simulated molecule at every moment. When it moves to the central region of the trap, the loading time t_{load} can be obtained. Then we fix the loading time and load all the molecules of the incident cold molecule beam; when $t = t_{\text{load}}$, we switch the loading electric field to the trapping one. When the number of the trapped molecules is stabilized, we can obtain the spatial and velocity distributions of cold molecules by counting the position and velocity of each molecule in the trapping region. The simulated results are shown in Figs. 7 and 8.

Figure 7(a) shows the dependence of the loading efficiency of cold molecules on the central velocity Vy_0 of the incident

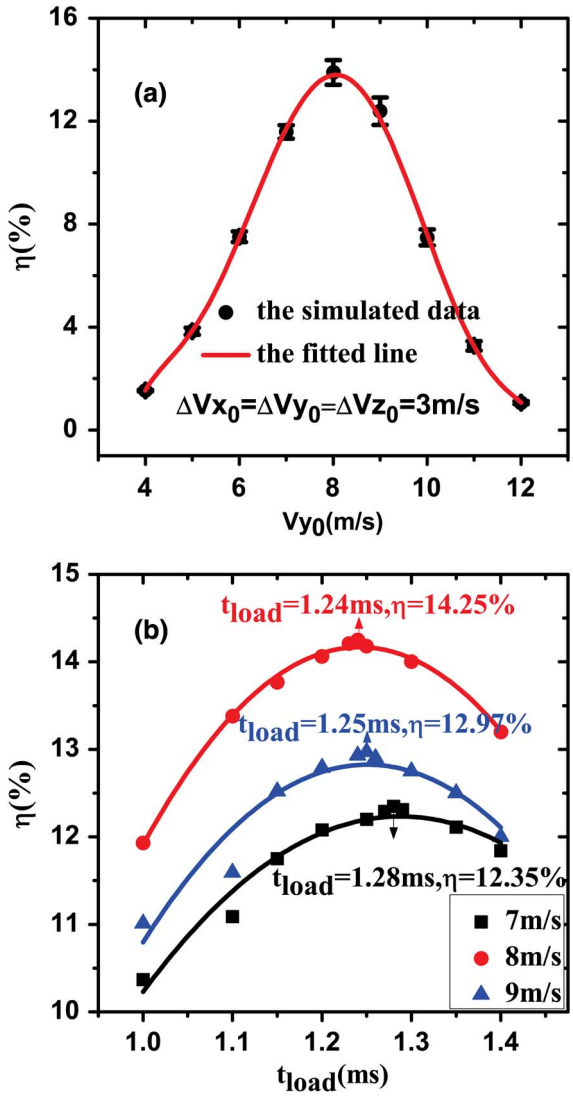

Fig. 7. Dependences of the loading efficiency of cold ND_3 molecules in the double-sphere combined with double-plate trap on both (a) the initial central velocity Vy_0 of incident ND_3 molecular beam for $Vx_0 = Vy_0 = Vz_0 = 3$ m/s and (b) the loading time t_{load} for different initial central velocities ($Vy_0 = 7$, 8, and 9 m/s). The data points are the simulated results, and the solid lines are the fitted curves.

molecular beam, and we find that the highest loading efficiency of cold molecules can reach ~14% when $Vy_0 = 8$ m/s. Figure 7(b) shows the dependence of the loading efficiency on the loading time, and we find that there is an optimal loading time for different initial central velocities of cold molecular beams; for instance, when $Vy_0 = 8$ m/s, we have $t_{load} = 1.24$ ms, which can provide a reliable theoretical basis for our further experimental study.

Figure 8 shows the initial and final velocity profiles of the loaded and trapped cold ND_3 molecules in our trap. It is clear from Fig. 8 that the velocity of cold molecules in the y direction is decelerated from 8 m/s to about 0 during the loading and trapping processes, and the FWHM of the final velocity distribution of the trapped cold molecules in the y direction and the corresponding temperature are about 7.80 m/s and 27.7 mK, respectively. We can also find that the FWHMs of the final velocity profiles in x and z directions are about 1.94 and 5.16 m/s, respectively, and the corresponding temperatures are about 1.71 and 13.8 mK; then the 3D temperature of the trapped cold molecules is about 19.2 mK. This shows that our proposed trap scheme can be used to realize an efficiently loading (~14% efficiency) and trapping of cold polar molecules with a temperature of ~20 mK.

B. Study of Optical-Potential Evaporative Cooling

As shown in Fig. 9, three pairs of laser beams can be arranged in x, y', and z' directions due to the open geometry of the trap. It is clear that such an electro-optical trap system has some important applications. For example, by using this system, we can load the optical traps for cold molecules, and then study the optical-potential evaporative cooling of cold molecules. In this case, cold polar molecules from an electrostatic Stark decelerator are first loaded into our proposed electrostatic trap. Afterward, one focused laser beam is propagated along the y' and another along the z' direction, and they are overlapped at the center of our electrostatic trap; and then cold molecules are loaded into a crossed optical dipole trap. Finally, the electric field is switched off after finishing the loading of cold molecules, and the optical-potential evaporative cooling of optically trapped cold molecules can be realized by lowering the trapping laser power; then an all-optical, chemically stabilized molecular Bose–Einstein condensate

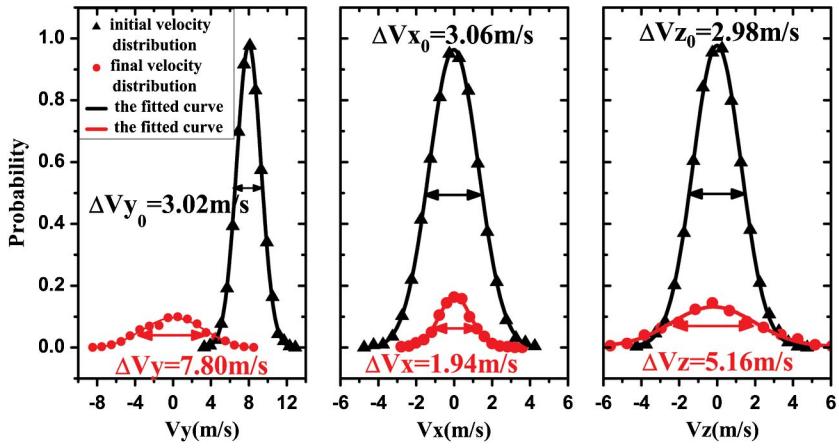

Fig. 8. Initial and final velocity distributions of cold ND_3 molecules in y, x, and z directions during the loading and trapping processes of the cold molecules in the double-sphere combined with double-plate trap. The data points are the simulated results, and the solid lines are the fitted curves.

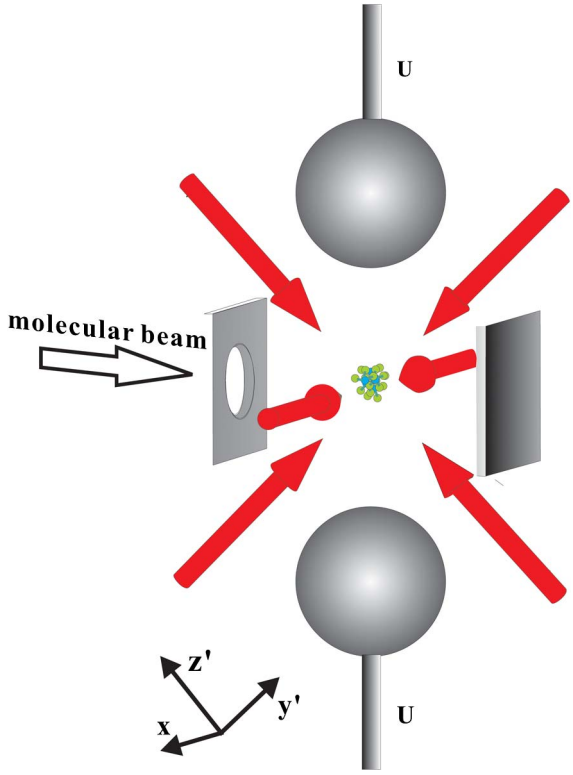

Fig. 9. Electro-optical trap system composed of three pairs of laser beams in x, y', and z' directions and an optically accessible electrostatic trap.

can be formed [27]. Also, if some polar molecules with an energy structure suitable to laser cooling and a pair of linearly Stark-split grounded-vibration and rotational levels can be found, our proposed optically accessible electrostatic trap can be used to realize laser cooling of neutral polar molecules in an electro-optical trap (EOT) with 3D optical molasses, which is similar to laser cooling of neutral atoms in a magneto-optical trap (MOT) [28].

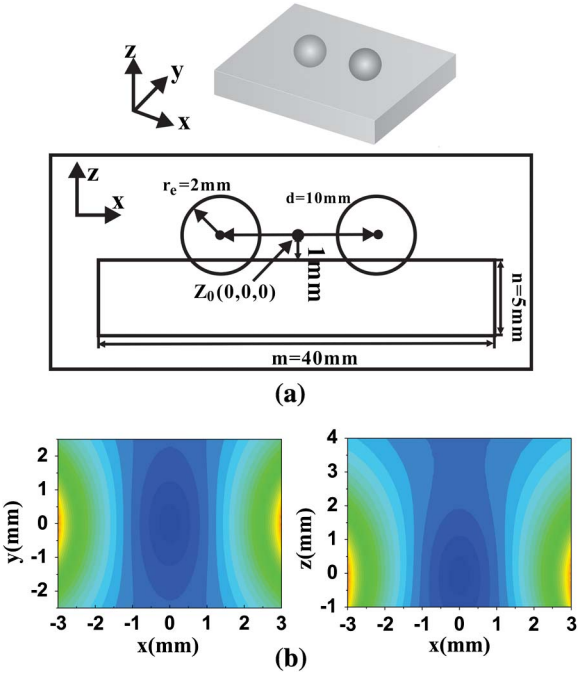

Fig. 10. (a) Schematic diagram of proposed electrostatic surface trap for cold polar molecules. (b) Contour distributions of the electrostatic field generated by our proposed surface trap in xoy and xoz planes for $r_e = 2$ mm, $d = 10$ mm and $U = 10$ kV.

C. Electrostatic Surface Trap

If our double-sphere trap is placed on the surface of an insulating Teflon ($\varepsilon_r = 2.2$) substrate, an electrostatic surface trap will be formed, as shown in Fig. 10(a). In our scheme, the two spherical electrodes with a radius of $r_e = 2$ mm are embedded into the substrate by 1 mm, and the distance between the centers of the two spheres is $d = 10$ mm, while the voltage applied to the electrodes is still $U = 10$ kV. In fact, the geometric sizes of our double-sphere layout can be further miniaturized to be several 10 μm, even to a few micrometers. We calculate the contour distributions of the electrostatic field generated by our surface trap layout in xoy and xoz planes, and the results are shown in Fig. 10(b). We can see that there is a 3D closed hollow electrostatic-field distribution on the surface of the substrate, which can be used to form an electrostatic surface trap for cold polar molecules in WFS states, and the trapping center is located at the position $(0, 0, -0.06)$, which is located above the surface of the substrate by about 0.94 mm.

5. CONCLUSIONS

We have proposed an optically accessible trap to catch cold polar molecules in WFS states by using two charged spherical electrodes, and we derived a set of analytical solutions to calculate the electric field distribution of our charged double-sphere layout. We have also studied the dependences of the electrostatic field and the Stark trapping potential for ND_3 molecules on both the radius of the spherical electrode and the distance between the centers of the two spheres, and we found that our proposed charged double-sphere scheme can be used to trap cold polar molecules in WFS states. In order to realize efficient loading of cold polar molecules, we have proposed a desirable scheme to load and trap cold molecules from a pulsed cold molecular beam by adding two plate-electrodes, and we studied the dependences of the loading efficiency on both the central velocity of an incident Stark-slowed ND_3 beam and the loading time by using a Monte Carlo method. Our study shows that the proposed double-sphere combined with double-plate scheme can be used to efficiently load and trap cold polar molecules in WFS states, and the maximal loading efficiency can reach ~14%.

Compared to other electrostatic trap schemes, our proposed double-sphere trap scheme has some unique advantages, such as a simple electrode structure and nearly completely open optical access, and it can be miniaturized and integrated on a chip, etc.; so our proposed electrostatic trap has some potential applications in integrated molecule optics and molecular chips, cold collisions [18,19], and cold chemistry [20], quantum computing and quantum information processing [21], and even optical-potential evaporative cooling of cold molecules, as well as the realization of an all-optical, chemically stabilized molecular Bose–Einstein condensate [27], and so on.

ACKNOWLEDGMENTS

We acknowledge Prof. Yingcheng Chen, Prof. Yangqin Chen and Hailing Wang, Dr. Yang Liu, Huirong Li, and Renqin Liu

for their helpful discussions. This work is supported by the National Natural Science Foundation of China under grants 10674047, 10804031, 10904037, 10974055, 11034002, and 11274114, the National Key Basic Research and Development Program of China under grants 2006CB921604 and 2011CB921602, the Basic Key Program of Shanghai Municipality under grant 07JC14017, and the Shanghai Leading Academic Discipline Project under grant B408.

REFERENCES

1. J. D. Weinstein, R. deCarvalho, T. Guillet, B. Friedrich, and J. M. Doyle, "Magnetic trapping of calcium monohydride molecules at millikelvin temperatures," Nature **395**, 148–150 (1998).
2. K. Maussang, D. Egorov, J. S. Helton, S. V. Nguyen, and J. M. Doyle, "Zeeman relaxation of CaF in low-temperature collisions with helium," Phys. Rev. Lett. **94**, 123002 (2005).
3. A. Fioretti, D. Comparat, A. Crubellier, O. Dulieu, F. Masnou-Seeuws, and P. Pillet, "Formation of cold Cs_2 molecules through photoassociation," Phys. Rev. Lett. **80**, 4402–4405 (1998).
4. C. Haimberger, J. Kleinert, M. Bhattacharya, and N. P. Bigelow, "Formation and detection of ultracold ground-state polar molecules," Phys. Rev. A **70**, 021402(R) (2004).
5. E. A. Donley, N. R. Claussen, S. T. Thompson, and C. E. Wieman, "Atom-molecule coherence in a Bose–Einstein condensate," Nature **417**, 529–533 (2002).
6. C. A. Regal, C. Ticknor, J. L. Bohn, and D. S. Jin, "Creation of ultracold molecules from a Fermi gas of atoms," Nature **424**, 47–50 (2003).
7. H. L. Bethlem, G. Berden, and G. Meijer, "Decelerating neutral dipolar molecules," Phys. Rev. Lett. **83**, 1558–1561 (1999).
8. H. L. Bethlem, F. M. H. Crompvoets, R. T. Jongma, S. Y. T. van de Meerakker, and G. Meijer, "Deceleration and trapping of ammonia using time-varying electric fields," Phys. Rev. A **65**, 053416 (2002).
9. T. Rieger, T. Junglen, S. A. Rangwala, G. Rempe, P. W. H. Pinkse, and J. Bulthuis, "Water vapor at a translational temperature of 1 K," Phys. Rev. A **73**, 061402(R) (2006).
10. Y. Liu, M. Yun, Y. Xia, L. Deng, and J. Yin, "Experimental generation of a cw cold CH_3CN molecular beam by a low-pass energy filtering," Phys. Chem. Chem. Phys. **12**, 745–752 (2010).
11. E. S. Shuman, J. F. Barry, D. R. Glenn, and D. deMille, "Radiative force from optical cycling on a diatomic molecule," Phys. Rev. Lett. **103**, 223001 (2009).
12. E. S. Shuman, J. F. Barry, and D. deMille, "Laser cooling of a diatomic molecule," Nature **467**, 820–823 (2010).
13. H. L. Bethlem, G. Berden, F. M. H. Crompvoets, R. T. Jongma, A. J. A. van Roji, and G. Meijer, "Electrostatic trapping of ammonia molecules," Nature **406**, 491–494 (2000).
14. W. C. Campbell, E. Tsikata, H.-I. Lu, L. D. van Buuren, and J. M. Doyle, "Magnetic trapping and Zeeman relaxation of NH ($X^3\Sigma^-$)," Phys. Rev. Lett. **98**, 213001 (2007).
15. T. Takekoshi, B. M. Patterson, and R. J. Knize, "Observation of optically cold cesium molecules," Phys. Rev. Lett. **81**, 5105–5108 (1998).
16. J. van Veldhoven, J. Küpper, H. L. Bethlem, B. Sartakov, A. J. A. van Roij, and G. Meijer, "Decelerated molecular beams for high-resolution spectroscopy," Eur. Phys. J. D **31**, 337–349 (2004).
17. E. R. Hudson, H. J. Lewandowski, B. C. Sawyer, and J. Ye, "Cold molecule spectroscopy for constraining the evolution of the fine structure constant," Phys. Rev. Lett. **96**, 143004 (2006).
18. K. Burnett, P. S. Julienne, P. D. Lett, E. Tiesinga, and C. J. Williams, "Quantum encounters of the cold kind," Nature **416**, 225–232 (2002).
19. J. L. Bohn, "Inelastic collisions of ultracold polar molecules," Phys. Rev. A **63**, 052714 (2001).
20. S. Willitsch, M. T. Bell, A. D. Gingell, S. R. Procter, and T. P. Softley, "Cold reactive collisions between laser-cooled ions and velocity-selected neutral molecules," Phys. Rev. Lett. **100**, 043203 (2008).
21. D. deMille, "Quantum computation with trapped polar molecules," Phys. Rev. Lett. **88**, 067901 (2002).
22. J. van Veldhoven, H. L. Bethlem, and G. Meijer, "AC electric trap for ground-state molecules," Phys. Rev. Lett. **94**, 083001 (2005).
23. J. van Veldhoven, H. L. Bethlem, M. Schnell, and G. Meijer, "Versatile electrostatic trap," Phys. Rev. A **73**, 063408 (2006).
24. M. Schnell, P. Lützow, J. van Veldhoven, H. L. Bethlem, J. Küpper, B. Friedrich, M. Schleier-Smith, H. Haak, and G. Meijer, "A linear AC trap for polar molecules in their ground state," J. Phys. Chem. A **111**, 7411–7419 (2007).
25. J. Kleinert, C. Haimberger, P. J. Zabawa, and N. P. Bigelow, "Trapping of ultracold polar molecules with a thin-wire electrostatic trap," Phys. Rev. Lett. **99**, 143002 (2007).
26. M. Kirste, B. G. Sartakov, M. Schnell, and G. Meijer, "Nonadiabatic transitions in electrostatically trapped ammonia molecules," Phys. Rev. A **79**, 051401(R) (2009).
27. J. Yin, "Realization and research of optically trapped quantum degenerate gases," Phys. Rep. **430**, 1–116 (2006).
28. E. L. Raab, M. Prentiss, A. Cable, S. Chu, and D. E. Pritchard, "Trapping of neutral sodium atoms with radiation pressure," Phys. Rev. Lett. **59**, 2631–2634 (1987).